Mechanical Switching of Ferroelectric Domains in 33-200 nm-Thick Sol-Gel-Grown PbZr 0.2 Ti 0.8 O 3 Films Assisted by Nanocavities

Sergio Gonzalez Casal, Xiaofei Bai, Kevin Alhada-lahbabi, Bruno Canut, Bertrand Vilquin, Pedro Rojo Romeo, Solène Brottet, David Albertini, Damien Deleruyelle, Matthieu Bugnet, et al.

Mechanical switching of ferroelectric domains in 33-200 nm thick sol-gel-grown $PbZr_{0.2}Ti_{0.8}O_3$ films assisted by nanocavities

Sergio Gonzalez Casal Xiaofei Bai Kevin Alhada-Lahbabi Bruno Canut Bertrand Vilquin Pedro Rojo Romeo Solène Brottet David Abertini Damien Deleruyelle Matthieu Bugnet Ingrid Canero Infante Brice Gautier**

Sergio Gonzalez Casal, Xiaofei Bai, Kevin Alhada-Lahbabi, Bruno Canut, Solène Brottet, David Abertini, Damien Deleruyelle, Ingrid Canero Infante, Brice Gautier
Address : Univ Lyon, INSA Lyon, CNRS, Ecole Centrale de Lyon, Université Claude Bernard Lyon 1, CPE Lyon, INL, UMR5270, 69621 Villeurbanne, France
Email Address : sergio.gonzalez-casal@insa-lyon.fr, brice.gautier@insa-lyon.fr
Bertrand Vilquin, Pedro Rojo Romeo
Address : Univ Lyon, Ecole Centrale de Lyon, CNRS, INSA Lyon, Université Claude Bernard Lyon 1, CPE Lyon, CNRS, INL, UMR5270, 69130 Ecully, France
Matthieu Bugnet
Address : Univ Lyon, CNRS, INSA Lyon, UCBL, MATEIS, UMR 5510, 69621 Villeurbanne, France

Keywords: *Ferroelectricity; Piezoresponse Force Microscopy; Ferroelectric switching; Lead Titanate Zirconate; Thin films*

The mechanical switching of ferroelectric domains is achieved in $PbZr_{0.2}Ti_{0.8}O_3$ thin films obtained by the sol-gel method for thicknesses up to 200 nm. The dielectric polarization can be switched when a force higher than a given threshold value in the order of some μNewtons is applied with the tip of an atomic force microscope. This threshold is determined as a function of the thickness of the films, and local hysteresis loops are recorded under mechanical stress. The possibility of switching the polarisation in such unusually thick films is related to the existence in their volume of physical nanoscale defects, which might play the role of pinning centers for the domains.

1 Introduction

Ferroelectric thin films have attracted a great deal of attention for their potential applications in electronic devices [1]. The possibility of switching between two stable states of dielectric polarization by the application of a low electric field is an ideal mechanism to design memories in digital electronics [2, 3]. It has been shown that the polarization could also be switched by the application of a mechanical stress, with or without electrical stimulation. This effect has been demonstrated in, *e.g.*, $BaTiO_3$[4, 5], $BiFeO_3$[6], and $PbZr_{0.2}Ti_{0.8}O_3$[7] or $PbZr_{0.52}Ti_{0.48}O_3$ [8].

Fine tuning the polarisation switching by combining electrical and mechanical excitation, or completely controlling it through a mechanical stress only would open the door to many applications related to stress detection or domain patterning. Beyond the

nature of the excitation, the material itself and its environment are of crucial importance to control of the domains when they are artificially created either by a mechanical or an electrical stimulus. Indeed, for a domain to be stable, it has to reach a minimal size and be clamped either on an electrode [9] or on charged defects [10]. Therefore, controlling the composition and the amount of defects in a ferroelectric thin film is key for the control of the stability of ferroelectric domains.

Among all ferroelectrics, $PbZr_xTi_{1-x}O_3$ is one of the most investigated materials and remains an ideal case study to gain insight into the mechanisms that govern the switching phenomena when a mechanical stress is involved. Specifically, the tetragonal structure of the $x = 0.2$ composition allows both large piezoelectric coefficients [11, 12, 13] and a good control of the desired orientation (perpendicular to the surface). This makes $PbZr_{0.2}Ti_{0.8}O_3$ (PZT) a material of choice to demonstrate the possible mechanical control of ferroelectric domains.

This work explores how polarization switching of ferroelectric domains can be controlled by the application of a mechanical stress on PZT thin films of thicknesses up to 200 nm. This is one of the largest thickness ever reported for which mechanical switching has been shown to be efficient. The presence of nanometer-size cavities underneath the surface, as observed by scanning transmission electron microscopy (STEM) images, are thought to be at the origin of the stabilization of ferroelectric domains created from the surface by the tip of an atomic force microscope (AFM).

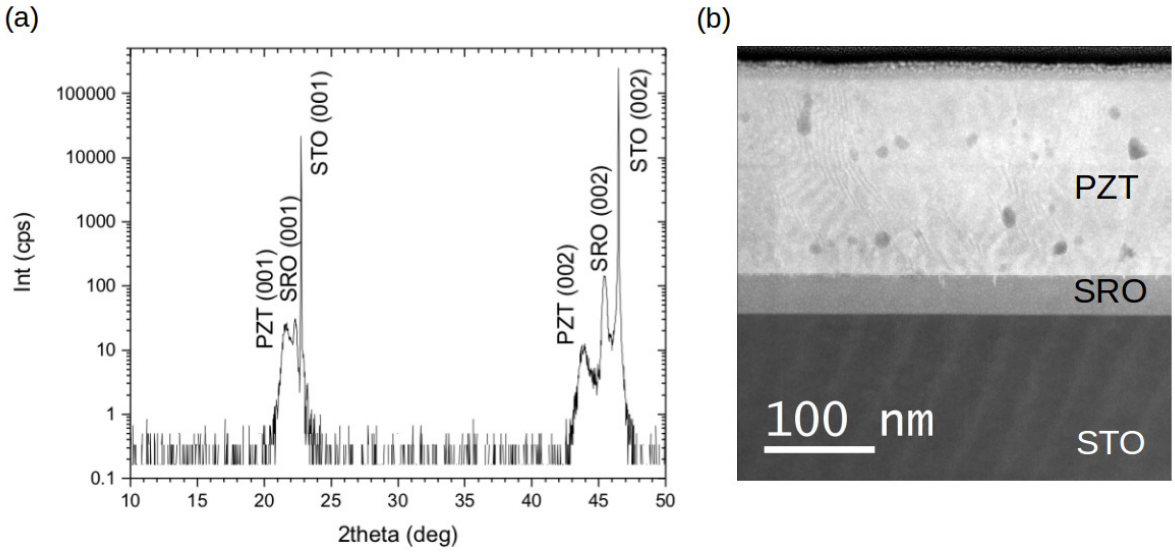

Figure 1: (a) $\theta - 2\theta$ XRD pattern of the 100 nm thick PZT film, indicating the corresponding reciprocal space lattice reflections for the PZT film, SRO electrode and STO substrate. (b) HAADF STEM overview of the 200 nm thick film. Cavities appear as dark areas inside the PZT layer.

2 Material and methods

A series of PZT thin films (thickness: 33, 66, 100 and 200 nm, hereafter named PZT_{33}, PZT_{66}, PZT_{100} and PZT_{200}), was obtained by the sol-gel spin coating route with a solution from Mitsubishi Materials, grown on a 30 nm thick $SrRuO_3$ (SRO) conductive layer used as a bottom electrode and deposited at 620°C on a $SrTiO_3$ (STO) single crystal substrate by radio frequency sputtering. The PZT crystalline phase is obtained after a rapid thermal annealing at 650°C under O_2 atmosphere for one minute. Samples with thicknesses up to 100 nm underwent a single crystallization annealing at the end of the deposition process. The thickest sample (PZT_{200}) was annealed once after the deposition of 100 nm of PZT, and a second time after the deposition of the additional 100 nm. One sample, referred as $PZT_{100,3c}$ underwent three crystallization annealing steps after each deposition step of $\simeq$ 33 nm-thick PZT layers.

The phase purity and crystal structure were checked by X-ray diffraction (XRD) using a Rigaku SmartLab diffractometer, equipped with a Cu-rotating anode using parallel beam and Ge(400) 2-bounce analyzer configuration to work under $Cu - K\alpha_1$ monochromatic radiation. The sol-gel grown thin films solely contain the tetragonal PZT phase, as evidenced by the XRD pattern of PZT_{100} shown in Figure 1a. The XRD pattern also shows that the PZT layer is entirely *c*-oriented, as indicated from (001) and (002) reflections for PZT, which means that the polarization is expected to be perpendicular to the sample's surface, either pointing towards the surface ("up" domains) or towards the substrate ("down" domains). This is the case for all films. The thickness of the PZT layers was measured by fitting the interference fringes around Bragg peaks (see supplementary material for details).

Cross section transmission electron microscopy lamellas were made by focused ion beam (FIB). High angle annular dark field (HAADF) imaging in STEM mode was performed using a Cs-corrected Jeol NeoARM operated at 200 kV. The thickness, as well as the structural and chemical homogeneity of the SRO and PZT layers were confirmed by STEM-HAADF imaging, as shown in Figure 1b for PZT_{200}.

Complementary characterization was obtained by Rutherford backscattering spectrometry (RBS) to quantitatively evaluate the atomic composition of the PZT layers and to measure their areal mass. The analysis was performed with $^4He^+$ ions of 2 MeV energy delivered by the 2 MV Van de Graaff accelerator of the SAFIR platform located at Paris Institute of Nanosciences. The backscattered ions were detected with a 13 keV resolution implanted junction set at an angle of 165° with respect to the beam axis. To improve the depth resolution on the thinnest layers and to depict a possible depth evolution of the film stoichiometry, RBS spectra were recorded under grazing incidence (75°) of the $^4He^+$ analysis beam.

Figure 2 shows the RBS spectrum recorded on a PZT sample of 100 nm nominal thickness. The signals related to Pb, Zr, and Ti are clearly visible. Within the analysis accuracy, no significant contamination from other atomic species of high atomic masses

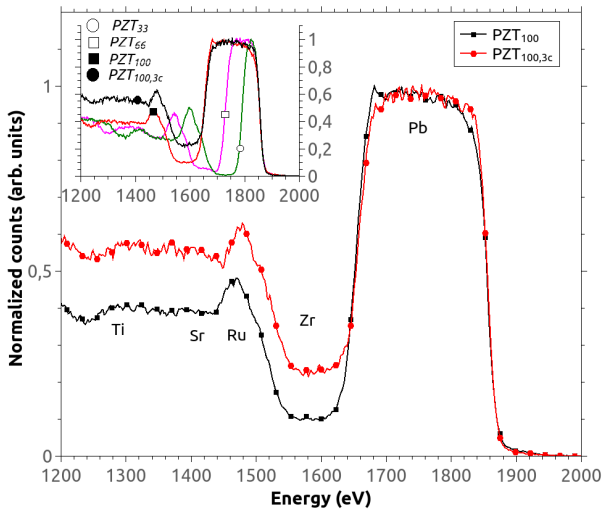

Figure 2: RBS spectra of PZT_{100} and $PZT_{100,3c}$ obtained at grazing incidence. Inset : RBS spectra of PZT_{33} and PZT_{66} shown with PZT_{100} and $PZT_{100,3c}$.

t (nm)	cryst.	d_A	d_V
33	1	21	6.36
66	1	44.5	6.74
100	1	71.5	7,15
100	3	67	6.70
166	2	95	7.14
200	2	147	7.35

Table 1: Areal density d_A ($\mu g/cm^2$) and volumic density d_V (g/cm^3) of all samples. d_V has been obtained by dividing d_A with the thickness of the sample.

can be detected in the film. With the help of a dedicated simulation code (SIMNRA software [14]), the average stoichiometry of $Pb_{0.20}Zr_{0.04}Ti_{0.16}O_{0.60}$ was extracted from the experimental data, in good agreement with the expected composition. The areal mass of the film was found to be 67 $mg.cm^{-2}$, corresponding to a film density equal to 90% of that of bulk PZT.

The characterization of ferroelectric domains was performed by dual frequency resonance tracking piezoresponse force microscopy (DFRT-PFM) using a Ntegra NT-MDT AFM with an external Zurich Instruments HF2LI system, which allows for the use of resonance tracking. Note that the AFM tip is always grounded and voltage applied on the sample's back electrode. More information about the setup can be found elsewhere [15] and in supporting information (Fig S1). The mechanical switching of domains was achieved using a Pt-Ir AFM tip with a spring constant of 4.6 ± 0.5 N/m for the two thinnest samples, and a doped diamond AFM tip with a spring constant of 90 ± 9 N/m for the two thicker ones. The spring constant was obtained through thermal noise calibration[16], while the force was calculated from different force curves measured over

the samples and applying Hooke's law [17].

2D phase-field simulations were conducted choosing the ferroelectric polarization (P_i, where $i = x, y$) as the order parameter with x and y being the horizontal and vertical upwards axis, respectively. The total free energy of the system is written as a function of the polarization P_i, the polarization gradient (∇P_i), the electric field (E_i) and the elastic strain (ϵ_{kl}):

$$F = \int \left[f_{landau}(P_i) + f_{domain}(\nabla P_i) + f_{elec}(P_i, E_i) + f_{elas}(P_i, \epsilon_{kl}) \right] d\vec{r} \tag{1}$$

with $d\vec{r} = dx\, dy$.

f_{landau}, f_{domain}, and f_{elas} are respectively the Landau, domain-wall (gradient) and the elastic energy density with their usual meanings [18]. More details and the description of each energy density term can be found in the supporting information. The effect of the stress gradient on polarization reversal is considered through a flexoelectric field acting as an additional contribution besides the electric field, as already proposed by Cao *et al.* [19] so that no chemical effect (*e.g.* Vegard strain) is taken into account. The flexoelectric field E_i^f was calculated using the flexocoupling coefficient tensor F_{ijkl} as [19]:

$$E_i^f = F_{ijkl} \frac{\partial \sigma_{ij}}{\partial x_l} \tag{2}$$

The electric contribution to the free energy (f_{elec}) is then written taking into account the electric and flexoelectric fields (E_i^s and E_i^f respectively). Denoting $\varphi(\mathbf{r})$ the electrostatic potential, the electric field ($\mathbf{E^s} = -\nabla\varphi$) is obtained by solving Poisson equation:

$$\nabla \cdot (-\varepsilon_0 \varepsilon_r(\mathbf{r}) \nabla\varphi(\mathbf{r}) + \mathbf{P}) = \rho_f(\mathbf{r}) \tag{3}$$

where ε_0 and $\varepsilon_r(\mathbf{r})$ are the vacuum and the local relative permittivity respectively and ρ_f the free charge density. f_{elec} is then expressed as:

$$f_{elec}(P_i, E_i) = -E_i \cdot P_i \quad \text{with } E_i = E_i^s + E_i^f \tag{4}$$

The temporal evolution of the ferroelectric polarization is computed using the time-dependent Landau-Ginzburg-Devonshire equation:

$$\frac{\partial P_i(\mathbf{r}, t)}{\partial t} = -L \frac{\delta F}{\delta P_i(\mathbf{r}, t)}, \quad i = x, y \tag{5}$$

where L is the kinetic coefficient related to the domain motion.

3 Results

3.1 Electrical and mechanical switching of domains

The complete electrical control of the domains, *i.e.*, the switching of the polarization state in either direction by applying a voltage, was possible for all samples with the

Pt-Ir coated tip. The coercive voltage increased with the thickness (from ±0.9 V to ±2 V for 33 nm to 100 nm, respectively), which is consistent with a decrease of the coercive field when the thickness is increased (from ±25 MV/m to ±20 MV/m for 33 nm thick and 100 nm thick samples respectively). For all thicknesses, the hysteresis loops were symmetrical, which means that the absolute value of the coercive voltage was the same for positive and negative applied voltages.

Mechanical switching of ferroelectric domains was achieved on fresh regions, which had not been previously electrically stressed to minimize any effects related with a possible charge injection. Note that the initial proportion of domains in each orientation varies with thickness. Indeed, PFM images of as-grown samples showed that a large majority of up domains is found in $33 - 100$ nm thick films, while the thickest sample (200 nm) had an equal proportion of "up" and "down" domains.

In order to quantitatively compare the PFM results obtained on samples with different thicknesses, only experiments performed with the very same tip are considered. Therefore, only the samples investigated with the soft cantilever and with a conductive tip (33 and 66 nm) will be compared. The same will apply for results obtained with a hard cantilever and with a diamond-coated tip (100 and 200 nm thick samples).

The phase and amplitude obtained by PFM when increasing the force while scanning with the AFM tip on the thinnest sample (33 nm) are shown in Figure 3a and b. The tip was moved from bottom to top while the applied force was increased stepwise. Five different forces were applied from 1.1 μN to 1.9 μN, as shown at the right hand side of Figure 3a. The topography profile shows no degradation of the surface due to the application of the force in this range. The genuine "up" polarization state in the thinnest samples (33 and 66 nm) appears dark in the PFM images. When the force exceeds a given threshold, the contrast of the PFM phase images turns bright, which indicates that the polarization has switched. For intermediate forces, switching is not total and some areas remain in the original state of polarization. Above a threshold force of $\simeq 1.6$ μN, the whole surface switches.

It must be noted that mechanical switching is possible only from up to down domains, because the mechanical stress induced by the tip is always applied from the surface, imposing a compressive stress.

The experimental procedure used for the thinnest layer was repeated for the 66 nm-thick sample (see Figure 3d), where forces ranging from 1.5 μN to 2.3 μN were applied. Compared to the 33 nm-thick sample, a larger force is needed to initiate domain switching, which is not observed below 2 μN. A second series of measurements was conducted to reach higher forces, from 1.9 μN to 2.7 μN, as shown in Figure 3g. In this second series, complete switching is achieved from 1.9 μN, which is comparable to the previous result considering the precision of the measurement of the tip stiffness.

For the thinnest sample, the amplitude image shows that where the switching is initiated, *i.e.*, where the applied force is slightly larger than the minimal force needed

to switch the domains, the global amplitude decreases due to a high density of small domains and domain walls (the amplitude is null at domain walls). When switching starts to be homogeneous, *i.e.*, the applied force is sufficient to switch the polarization everywhere, the amplitude increases again. This behavior is similar to that reported on a 4.8 nm-thick epitaxial $BaTiO_3$ film [4]. Nevertheless, this phenomenon is hardly visible for the 66 nm-thick sample.

From PFM images, it is possible to compute the proportion of domains that switched after the application of the stress by binarizing the phase images and computing the number of pixels in the up and down state in every region. The binarization was performed with a dedicated software (Gwyddion [20]). Figure 4a and 4b show the percentage of switched area as a function of the force for four samples with thicknesses ranging from 33 nm to 200 nm. Defining arbitrarily the threshold force F_t as the force needed to switch at least 75% of the domains of a sample of thickness t, we find : $F_{33nm} = 1.6$ μN, $F_{66nm} = 2.3$ μN, $F_{100nm} = 20.9$ μN, and $F_{200nm} = 31.5$ μN. Note that F_{33nm} and F_{66nm} were obtained with the soft cantilever, while F_{100nm} and F_{200nm} were obtained with the hard cantilever. Therefore, it can only be concluded that the threshold force increases from the 33 nm to the 66 nm thick sample, and from the 100 nm to the 200 nm sample, which suggests that an increase of the threshold force with the thickness of the sample is a reasonnable hypothesis.

The experiment with the hard tip was also performed with the PZT_{33} sample to compare the value obtained with the soft tip. In this case, F_{33} $nm = 8.5$ μN. To compare the force thresholds obtained, Hertz's model [21] was applied to compute a pressure threshold instead of a force threshold. Figure 4 shows the evolution of the pressure threshold with the thickness, which evolves linearly. It should be noted that the pressure thresholds obtained for the thinnest sample with both the hard and soft tips are similar.

Hysteresis loops were performed on the 33 nm-thick film for different applied forces in order to evaluate the evolution of the coercive voltage, as shown in Figure 5. The coercive voltage shifts toward positive values as the mechanical stress increases, and the lower value of the coercive voltage becomes positive for an applied force higher than 1.7 μN, which indicates that the opposite polarisation state is not stable in the absence of applied electric field.

To complete this study, hysteresis loops obtained with a 1.4 μN applied force were recorded at several locations on the surface of the sample, as shown in Figure 6. The same shift is observed at every location where a domain has been permanently created (square and circle in Figure 6), whereas the hysteresis loop remains symmetric in the regions where no switching is obtained (diamond marker) . Therefore, switching is not systematically obtained for the same applied force, and the shift of the loop happens every time switching is effective.

3.2 Influence of the growth process

The ability of the layer to be switched mechanically has been compared for two samples of the same thickness (100 nm) with either a single or three crystallization steps: PZT_{100} and $PZT_{100,3c}$.

From Figure 7, the force needed to switch the domains mechanically is significantly lower when the samples have been annealed three times.

Figure 8a shows STEM-HAADF images of PZT_{100}. Nanometer-size cavities are present in the volume of both films, although they seem to be located closer to the surface in the case of $PZT_{100,3c}$ compared to PZT_{100} where they lie close to the interface with SRO. Such cavities are observed in all samples, irrespective of their thickness. The proportion of cavities in the layer along with the average area of the cavities have been computed and are represented in Figure 8b and c respectively. Considering that PZT_{200} has been annealed twice during the growth process, it is clear from this graph that the percentage of cavities is linked to the number of crystallizations that have been used, regardless of the thickness of the layers. To this length, Figure 8b) shows that all films that have undergone a single crystallisation share the same proportion of cavities (between 1.4 and 2.3 %), whereas the films that have been annealed two or three times show a percentage of cavities of 3.4% and 5.6 %, respectively. Moreover, the average size of the cavities seems to increase monotonously with the thickness of the PZT film, regardless of the number of crystallizations, as shown in Figure 8c. The dependence of the cavity size and density on the thickness clearly suggests that the cavities are essentially created by the sol-gel crystallization process, and excludes a major influence of the FIB preparation process of the TEM lamellae. It is worth noting that the RBS analysis (Figure 2) shows that the base signal (from all species except Pb) is different for PZT_{100} and $PZT_{100,3c}$, and corresponds to a $\simeq 4.2$ % lower density in $PZT_{100,3c}$ (see Table 1). This variation is very close to the difference in the percentage of cavities computed from STEM-HAADF images in layers that have undergone one or three crystallizations.

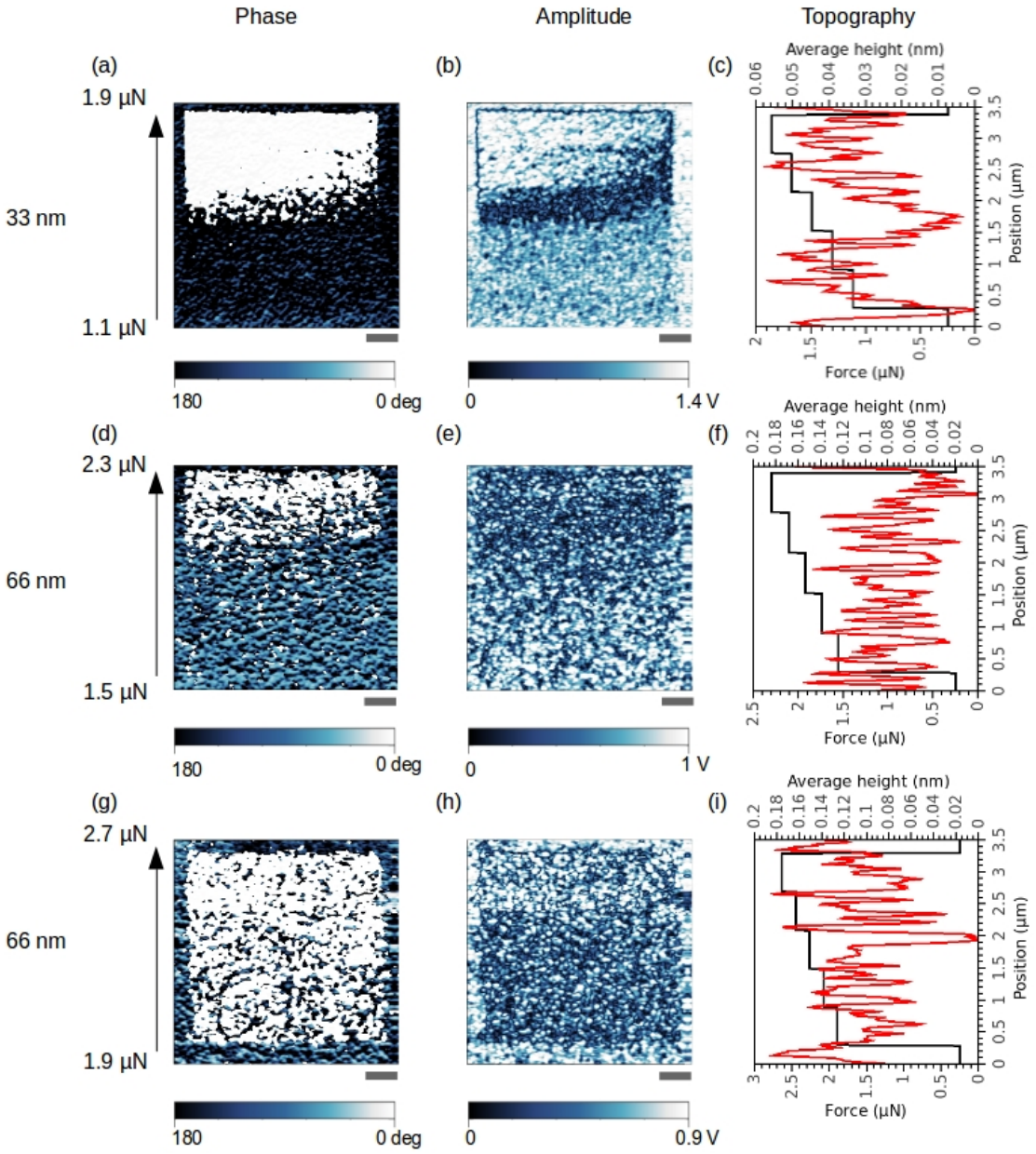

Figure 3: Ferroelectric domain switching using mechanical stress for PZT samples of 33 nm and 66 nm thickness (a), (d) and (g) phase image (b), (e) and (h) amplitude image and (c), (f) and (i) section profile and force plot. The gray line at the bottom right corner of the images represents 500 nm . The spatial evolution of the applied force (black solid line) is shown alongside the topography (red solid line), as a function of the vertical tip position. The total acquisition time of each image was 12 min 48 seconds. A Pt-Ir tip was used.

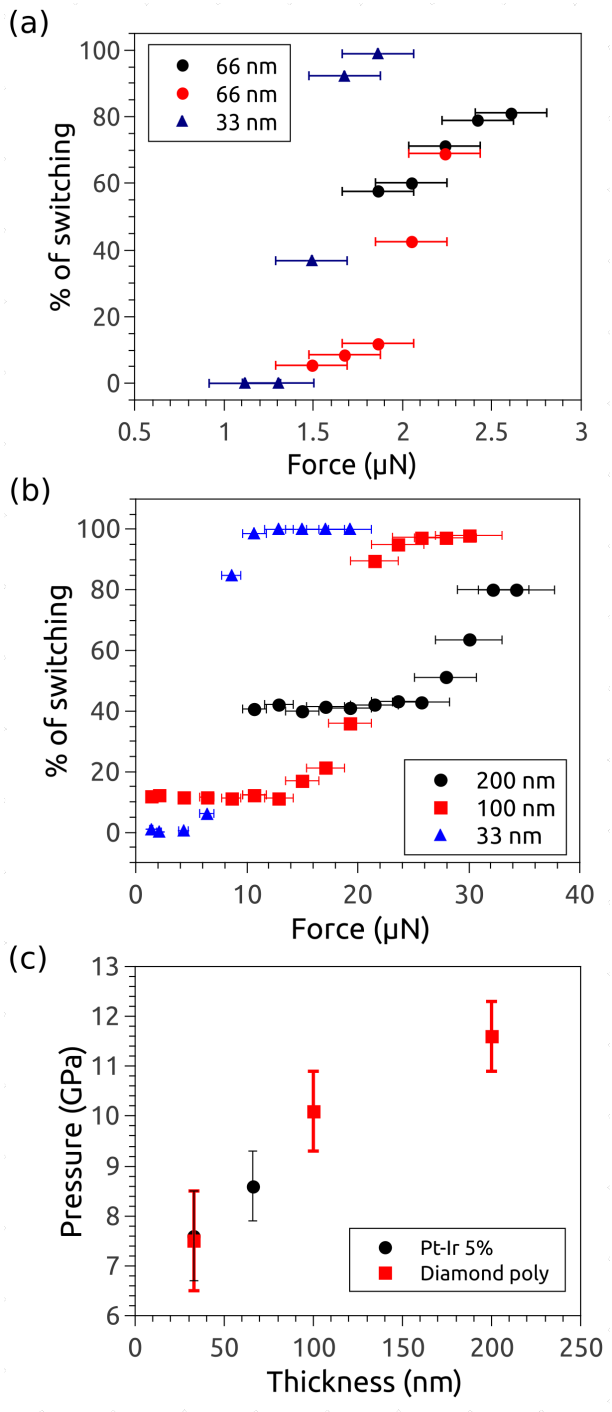

Figure 4: (a) and (b) : evolution of the switching probability (expressed as the percentage of switched domains) as a function of the force applied by the AFM tip, for two differents series of thicknesses. (c) Pressure threshold as a function of the thickness of the layers.

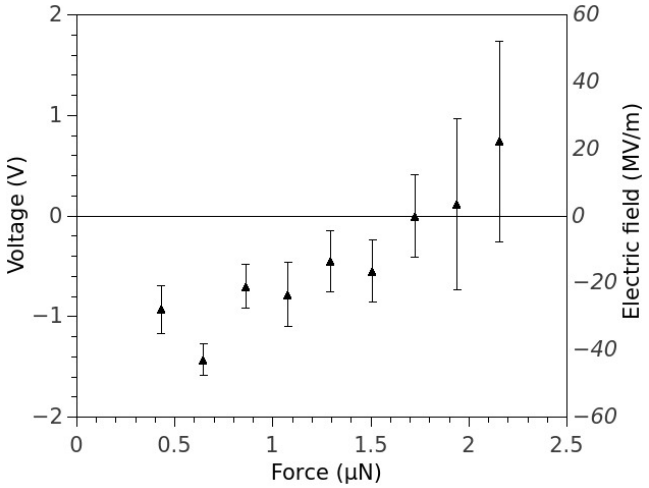

Figure 5: Evolution of the coercive voltage and corresponding coercive electric field for the up to down switching as a function of the applied force for the 33 nm thick film. Coercive voltage values are obtained from the minimum amplitude of the PFM hysteresis loops.

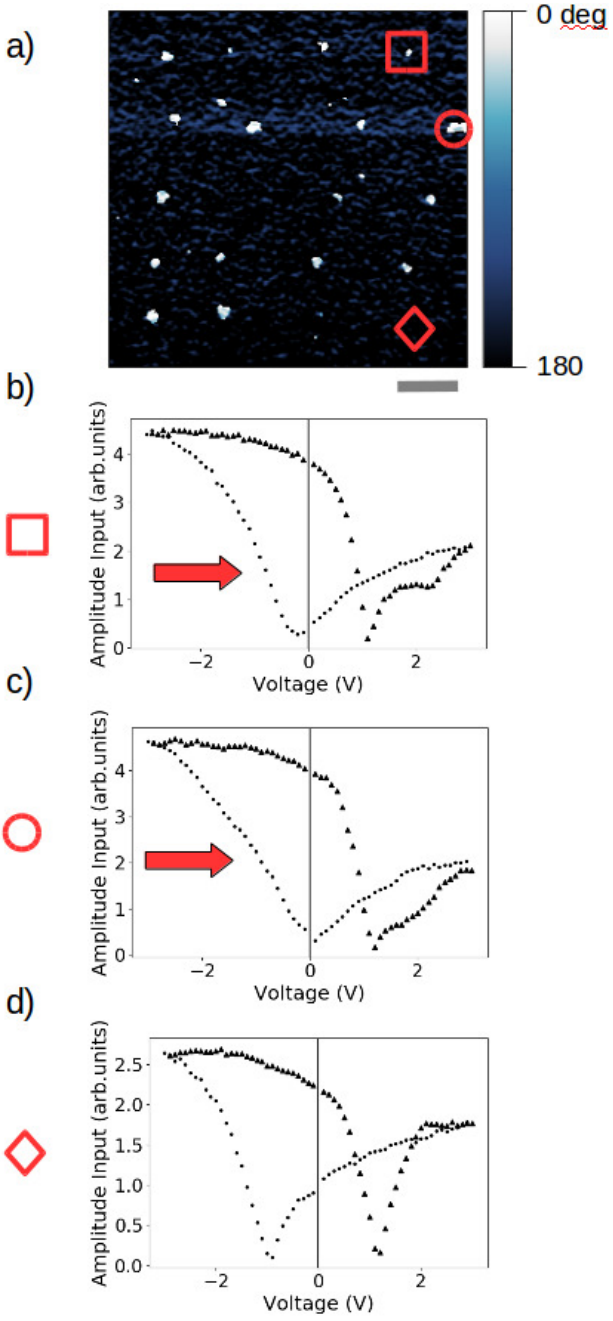

Figure 6: Hysteresis loops obtained at different locations with the same force of 1.4 μN. (a) Phase image of the ferroelectric domains after switching experiments have been conducted at 20 different locations, scalebar is 500 nm. (b-d) PFM amplitude loops obtained on the area marked with a square, circle and diamond respectively. Red arrows indicate the direction of the shift of the loops with respect to the symmetrical position.

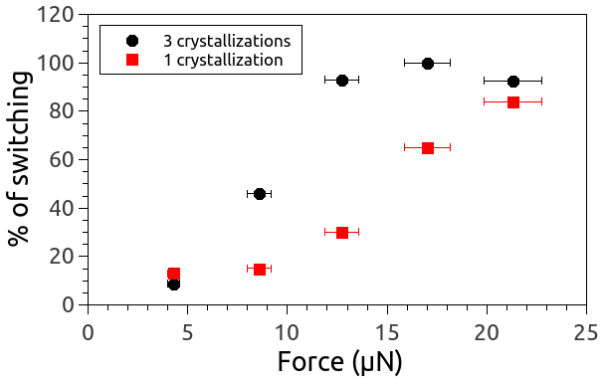

Figure 7: Proportion of switched domains as a function of the applied force for two 100 nm thick PZT samples that have been annealed once or three times.

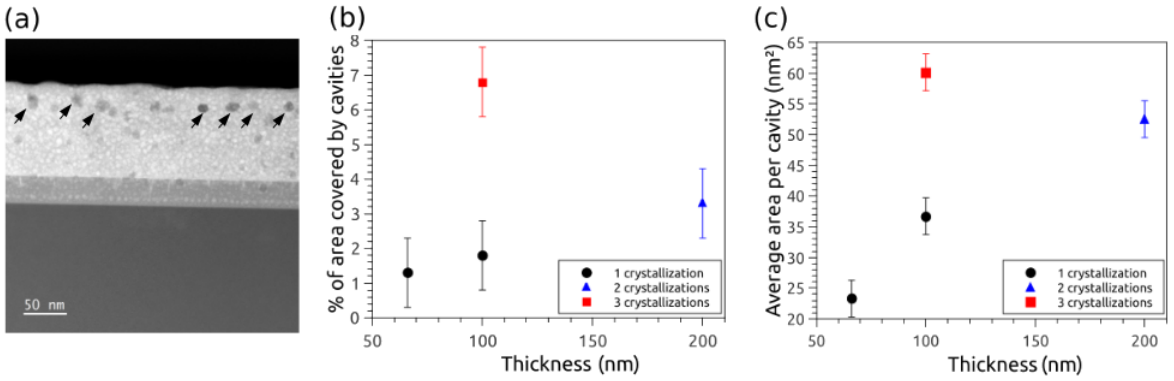

Figure 8: a) TEM image of a cross section of sample PZT_{100}. Dark arrows point to the cavities. b) Proportion of cavities and c) average size of cavities as a function of the thickness of the films.

4 Discussion

The evolution of the coercive voltage with the applied force in Figure 5 describes the switching process. Starting from up domains (upper state in the hysteresis loop), the application of the pressure shifts the hysteresis loop until the up state is not stable anymore at zero applied electric field. For a 1.7 μN applied force, the lower negative coercive voltage becomes positive, forcing the polarization to switch to a down state. When the pressure is released, the polarization stays in that state.

The shift of the hysteresis loop is consistent with the appearance of a fixed electric field in the layer. This electric field can be created by the flexoelectric effect (thus related to the stress gradient) or bulk electrochemical effects [22]. The large strain imposed by the AFM tip applying a few μN over a very small surface leads to a huge non-uniform stress, and either to a possible large electric field created from flexoelectricity [23], or to a high degree of mobility of ionic species like oxygen vacancies [24, 25, 26], which contributes to the onset of the electric field. This is consistent with the fact that the polarization can only be reversed in a unique direction : only compression is possible with an AFM tip, and the created electric field is always in the same direction.

The ferroelectric domains observed by PFM are stable, suggesting that they are clamped somewhere in the structure and that they do not switch back to their original state of polarisation. For clamping to be possible, compensation charges must be brought so that the polarisation charge is compensated to allow the depolarisation field to decrease. This can happen when the ferroelectric domain propagates from the top electrode down to the bottom electrode [9], where compensation charges are available in sufficient number to fully counterbalance the polarisation charge. As mentioned earlier, one of the possible mechanisms that could be responsible for the observed mechanical switching is the flexoelectric effect, which relates the gradient of the stress to the appearance of an electric field. However in that case, it is likely that the distribution of the electric field decreases very quickly with depth [22, 23], which would not allow the domains that are switched in this way to propagate deep enough in the film and be clamped on the bottom electrode when the layer is too thick. Therefore, the flexoelectric effect should not be efficient for films thicker than 20 nm, which is thinner than the thinnest of our films [27], unless the domains created by such a mechanism are clamped before they reach the bottom electrode.

Even in the case where switching for such large thicknesses is obtained through bulk phenomena (Vegard stress [26, 28], migration of oxygen vacancies [29, 30, 26]), a pinning mechanism should be in play to explain how mechanically switched ferroelectric domains can be obtained in such thick films. Indeed, the present results demonstrate the switching of PZT films as thick as 200 nm, which is a major difference with existing reports, where switching was only demonstrated for layers up to 100 nm or less [7, 22, 23].

Our results suggest that the ferroelectric domains, irrespective of the underlying

mechanism responsible for their stability, are clamped in the volume of the layer, possibly by defects. Although the growth of PZT thin films by soft chemical methods like sol-gel is not very common, despite the advantage of it being an affordable synthesis process to coat large areas, the presence of nanoscale cavities has been reported recently in similar films grown by metalloorganic decomposition [31]. The low magnification STEM-HAADF images in Figure 1b and in Figure 8 show that films do have a large amount of such nanometer-size defects, the aforementioned cavities, which could favor the clamping of domains created by the flexoelectric effect, without the need to reach the bottom electrode. The same might be true if the domains are created by bulk electro-chemical effects. Thus, the hypothesis of domains not reaching the bottom electrode seems the most probable. Such shallow domains can still be detected by PFM, because the contribution of surface domains dominates the response.

Phase field simulations have been conducted in order to confirm that the proposed scenario can adequately describe the experiments. The effect of nanometer-sized cavities enclosed in the ferroelectric film was evaluated through these simulations by considering circular paraelectric inclusions having the same dielectric constant as the PZT layer. In a first sequence, the pressure was applied locally over an adjustable time window (in the microsecond range), which leads to the switching of the domains under the tip due to the flexoelectric effect and to the growth of a switched domain starting from the apex of the tip and progressing in the vertical direction towards the back electrode. Then, pressure was released and the simulation ran until a steady state is reached. When no cavity is present in the volume of the layer, the switched ferroelectric domain disappears if it has not reached the bottom electrode before the stress is released. Otherwise, it is stable and a switched domain crosses the whole layer (see Figure 9, left). When a small cavity is induced, modeled as a paraelectric material, the switched domain created during the application of the pressure remains stable when it has reached the cavity (see Figure 9, right). This simple model appears to confirm that defects like voids or paraelectric phases embedded in the ferroelectric material can stabilize domains of opposite polarisation, and would explain why it remains possible to switch domains by mechanical stress even in the case of relatively thick layers as in our experiments, where domains can be clamped on the cavities.

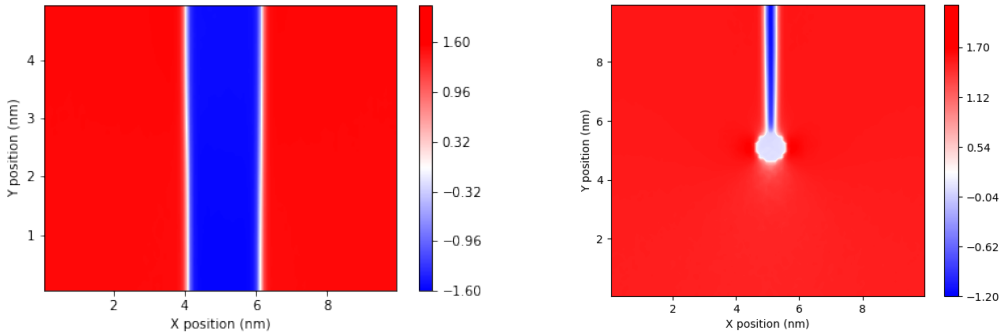

Figure 9: Phase field simulation of the growth of ferroelectric domains under the action of the flexoelectric effect. Left : the pressure has been applied long enough to let the domain grow down to the bottom electrode : the switched domain is clamped. Thickness of the film : 5 nm. Right : when a cavity is present, the domain is clamped on the cavity. Thickness of the film : 10 nm. The color scale refers to the value of the polarisation in arbitray units : red and blue regions stand for opposite polarisations.

5 Conclusions

In conclusion, the control of ferroelectric domains with mechanical stress was evidenced for $PbZr_{0.2}Ti_{0.8}O_3$ films of thicknesses up to 200 nm . The switching from up to down polarization was possible by applying a sufficiently high mechanical stress and without any applied voltage. The switching is characterized by the shift of the hysteresis loop, suggesting the onset of an internal electric field created by the mechanical stress. Large (5-10 nm diameter) defects of low atomic density, namely cavities, were created during the growth process and observed in the films using STEM-HAADF imaging. Their size increases monotonously with the thickness of the films, and their density is linked to the number of crystallizations carried out during the sol-gel process. These cavities might play the role of pinning centers for the domains, allowing them to be clamped without reaching the bottom electrode.

References

[1] J. F. Scott, C. A. Paz de Araujo, Ferroelectric Memories, Science 246 (4936) (1989) 1400–1405, publisher: American Association for the Advancement of Science. doi:10.1126/science.246.4936.1400.

[2] P. Sharma, D. Sando, Q. Zhang, X. Cheng, S. Prosandeev, R. Bulanadi, S. Prokhorenko, L. Bellaiche, L. Chen, V. Nagarajan, J. Seidel, Conformational Domain Wall Switch, Advanced Functional Materials 29 (18) (2019) 1807523. doi:10.1002/adfm.201807523.

[3] A. Crassous, T. Sluka, A. K. Tagantsev, N. Setter, Polarization charge as a reconfigurable quasi-dopant in ferroelectric thin films, Nature Nanotechnology-doi:10.1038/nnano.2015.114.

[4] H. Lu, C. W. Bark, D. Esque De Los Ojos, J. Alcala, C. B. Eom, G. Catalan, A. Gruverman, Mechanical writing of ferroelectric polarization, Science 335 (6077) (2012) 59–61.

[5] B. Wang, H. Lu, C. W. Bark, C. B. Eom, A. Gruverman, L. Q. Chen, Mechanically induced ferroelectric switching in $BaTiO_3$ thin films, Acta Materialia 193 (2020) 151–162. doi:10.1016/j.actamat.2020.04.032.

[6] S. M. Park, B. Wang, S. Das, S. C. Chae, J. S. Chung, J. G. Yoon, L. Q. Chen, S. M. Yang, T. W. Noh, Selective control of multiple ferroelectric switching pathways using a trailing flexoelectric field, Nature Nanotechnology 13 (5) (2018) 366–370. doi:10.1038/s41565-018-0083-5.

[7] E. J. Guo, R. Roth, S. Das, K. Dörr, Strain induced low mechanical switching force in ultrathin PbZr 0.2 Ti 0.8 O 3 films, Applied Physics Letters 105 (1) (2014) 0–5. doi:10.1063/1.4889892.

[8] G. Vats, Ravikant, P. Schoenherr, A. Kumar, J. Seidel, Low-pressure mechanical switching of ferroelectric domains in pbzr0.48ti0.52o3, Advanced Electronic Materials 6 (10) (2020) 2000523. doi:https://doi.org/10.1002/aelm.202000523.

[9] A. Brugère, S. Gidon, B. Gautier, Finite element method simulation of the domain growth kinetics in single-crystal $litao_3$: Role of surface conductivity, Journal of Applied Physics 110 (5) (2011) 052016. doi:10.1063/1.3623762.

[10] Y. Kitanaka, Y. Noguchi, M. Miyayama, Oxygen-vacancy-induced 90 degrees-domain clamping in ferroelectric bi4ti3o12 single crystals, Phys. Rev. B 81 (2010) 094114. doi:10.1103/PhysRevB.81.094114.

[11] E. Cattan, J. F. Manceau, T. Haccart, S. Biwersi, G. Velu, D. Remiens, F. Bastien, Remanent piezoelectric constant of PZT thin films, Ferroelectrics 224 (1-4) (1999) 307–314. doi:10.1080/00150199908210581.

[12] D. L. Polla, L. F. Francis, Processing and characterization of piezoelectric materials and integration into microelectromechanical systems, Annual Review of Materials Science 28 (1) (1998) 563–597. doi:10.1146/annurev.matsci.28.1.563.

[13] F. Xu, S. Trolier-McKinstry, W. Ren, B. Xu, Z. L. Xie, K. J. Hemker, Domain wall motion and its contribution to the dielectric and piezoelectric properties of lead zirconate titanate films, Journal of Applied Physics 89 (2) (2001) 1336–1348. doi:10.1063/1.1325005.

[14] M. Mayer, Simnra, a simulation program for the analysis of nra, rbs and erda, AIP Conference Proceedings 475 (1) (1999) 541–544. doi:10.1063/1.59188.

[15] S. Guillemin, R. Parize, J. Carabetta, V. Cantelli, D. Albertini, B. Gautier, G. Bremond, D. Fong, H. Renevier, V. Consonni, Quantitative and simultaneous analysis of the polarity of polycrystalline ZnO seed layers and related nanowires grown by wet chemical deposition, Nanotechnology.

[16] J. L. Hutter, J. Bechhoefer, Calibration of atomic-force microscope tips, Review of Scientific Instruments 64 (7) (1993) 1868–1873. doi:10.1063/1.1143970.

[17] B. Cappella, G. Dietler, Force-distance curves by atomic force microscopy, Surface Science Reports 34 (1) (1999) 1–104. doi:https://doi.org/10.1016/S0167-5729(99)00003-5.

[18] Y. L. Li, S. Y. Hu, Z. K. Liu, L. Q. Chen, Effect of electrical boundary conditions on ferroelectric domain structures in thin films, Applied Physics Letters 81 (3) (2002) 427–429. arXiv:https://doi.org/10.1063/1.1492025, doi:10.1063/1.1492025. URL `https://doi.org/10.1063/1.1492025`

[19] Y. Cao, Q. Li, L. Q. Chen, S. V. Kalinin, Coupling of electrical and mechanical switching in nanoscale ferroelectrics, Applied Physics Letters 107 (20). doi:10.1063/1.4935977.

[20] D. Nečas, P. Klapetek, Gwyddion: an open-source software for SPM data analysis, Central European Journal of Physics 10 (2012) 181–188. doi:10.2478/s11534-011-0096-2.

[21] T. D. B. Jacobs, C. Mathew Mate, K. T. Turner, R. W. Carpick, Understanding the Tip–Sample Contact, John Wiley and Sons, Ltd, 2013, Ch. 2, pp. 15–48. doi:https://doi.org/10.1002/9781118723111.ch2.

[22] Y. Cao, A. Morozovska, S. V. Kalinin, Pressure-induced switching in ferroelectrics: Phase-field modeling, electrochemistry, flexoelectric effect, and bulk vacancy dynamics, Physical Review B 96 (18) (2017) 184109.

[23] Y. Gu, Z. Hong, J. Britson, L.-Q. Chen, Nanoscale mechanical switching of ferroelectric polarization via flexoelectricity, Applied Physics Letters 106 (2) (2015) 022904. doi:10.1063/1.4905837.

[24] Y. Gil, O. M. Umurhan, I. Riess, Properties of a solid state device with mobile dopants: Analytic analysis for the thin film device, Journal of Applied Physics 104 (8). doi:10.1063/1.2993618.

[25] C. Ferreyra, M. Rengifo, M. J. Sánchez, A. S. Everhardt, B. Noheda, D. Rubi, Key Role of Oxygen-Vacancy Electromigration in the Memristive Response of Ferroelectric Devices, Physical Review Applied 14 (4) (2020) 1. arXiv:2006.10891, doi:10.1103/PhysRevApplied.14.044045.

[26] S. Das, B. Wang, Y. Cao, M. Rae Cho, Y. Jae Shin, S. M. Yang, L. Wang, M. Kim, S. V. Kalinin, L. Q. Chen, T. W. Noh, Controlled manipulation of oxygen vacancies using nanoscale flexoelectricity, Nature Communications 8 (1) (2017) 1–8. doi:10.1038/s41467-017-00710-5.

[27] P. Zubko, G. Catalan, A. K. Tagantsev, Flexoelectric Effect in Solids, Annual Review of Materials Research 43 (1) (2013) 387–421. doi:10.1146/annurev-matsci-071312-121634.

[28] A. R. Denton, N. W. Ashcroft, Vegard's law, Physical Review A 43 (6) (1991) 3161–3164. doi:10.1103/PhysRevA.43.3161.

[29] Y. Heo, D. Kan, Y. Shimakawa, J. Seidel, Resistive switching properties of epitaxial BaTiO3-δ thin films tuned by after-growth oxygen cooling pressure, Physical Chemistry Chemical Physics 18 (1) (2016) 197–204. doi:10.1039/c5cp05333a.

[30] P. Sharma, Z. Huang, M. Li, C. Li, S. Hu, H. Lee, J. W. Lee, C. B. Eom, S. J. Pennycook, J. Seidel, Ariando, A. Gruverman, Oxygen Stoichiometry Effect on Polar Properties of LaAlO3/SrTiO3, Advanced Functional Materials 28 (23) (2018) 1–8. doi:10.1002/adfm.201707159.

[31] T. Kiguchi, T. Shimizu, T. Shiraishi, T. J. Konno, Epitaxial growth mechanism of pb (zr, ti) o3 thin films on srtio3 by chemical solution deposition via self-organized seed layer, Journal of the Ceramic Society of Japan 128 (8) (2020) 501–511.

Supporting Information

See supplementary material for the full description of sol-gel process and x-ray diffraction characterization as well as studies about the initial distribution of domains in the samples and images of the switching in the 100 and 200 nm samples.

The data that support the findings of this study are available from the corresponding author upon reasonable request.

Supporting Information is available from the Wiley Online Library or from the author.

Acknowledgements

SGC acknowledges PhD funding from the Ministère de l'Enseignement Supérieur et de la Recherche, in the framework of Enjeux INSA Lyon. The authors acknowledge access to the NanoLyon platform for thin film synthesis. The STEM work was performed at the consortium Lyon-St-Etienne de microscopie. MB, ICI and BG acknowledge funding from INSA Lyon (grant BQR TORNADO), IngeLySE (grant CONIFER). This work was carried out thanks to the financial support of the IDEXLYON Project of University of Lyon as part of the Investments for the Future Program (ANR-16-IDEX-0005) through the granted FERLIGHT project.